

track down. The main difficulty lies perhaps in the preparation and characterization of the sample itself. There are many ways to prepare what has been called "glassy water," including the deposition of water vapor on a cold substrate (4), the preparation of an amorphous solid by applying pressure to crystalline ice at low temperatures (which yields a high-density form of amorphous ice) and then annealing this material to obtain a low-density amorphous ice (5), and the very rapid cooling (at rates of  $\sim 10^6$ °C/s) of liquid water to obtain a glassy solid (6). The glass transition temperature can be determined by warming these samples and observing either thermodynamic behavior characteristic of the glass transition (7) (see the figure) or measurable liquidlike behavior.

Experimental measurement techniques include calorimetry, diffusion, and macroscopic flow measurements (8). In these data, it is often difficult to distinguish a glass transition from other phenomena occurring in the solid phase. Theoretical studies typically use molecular dynamics studies to identify a liquidlike diffusion constant from mean-squared displacements of particles. Here, the main difficulty is that the glass transition depends on the interatomic potential used to describe interactions between water molecules at low temperatures. Another more fundamental problem is that the materials made by vapor deposition or annealing of pressurized materials

may not be related to a glass at all (9). Also, different forms of the amorphous ice can yield different values for the glass transition temperature (10).

From their analysis of thermodynamic data, Velikov *et al.* (1) conclude that the glass transition temperature in water is almost 30 K above the currently accepted value of about 136 K. The authors analyze data on hyperquenched glassy water obtained from the use of a differential scanning calorimeter. This is a very reasonable choice because this sample is most likely a true glass. On the basis of a simple replotting of the calorimetric data of Johari *et al.* (10), the authors suggest that if the glass transition temperature for water is the accepted value of  $\sim 136$  K, liquid water data would be quite anomalous compared with a number of other glasses. Only when the transition temperature is about 165 K do the replotted data for water look normal.

These results may have a substantial impact on the study of the phase behavior of water. If the transition temperature must indeed be relocated to 165 K, then studies of the glass transition will become even more difficult because crystallization is harder to avoid at this temperature. Furthermore, there are suggestions in the literature that water undergoes a transition from a "strong" to a "fragile" liquid (11) around 140 K. For a strong liquid, the logarithm of the viscosity changes linearly with the inverse of temperature, whereas

the viscosity of a fragile liquid shows a steep drop over a narrow temperature range. If water is not a liquid at 140 K, then this picture will change substantially. Our understanding of the behavior of water in microporous materials and in contact with biological materials at low temperatures would also change.

If Velikov *et al.*'s results are correct, then there is a new region in the water phase diagram where the material differs from the low-temperature glass and the high-temperature liquid. Their analysis will likely be controversial and stimulate new research on the search for the elusive glass transition temperature in water. For example, the use of pressure may help to avoid crystallization and identify the "true" glass transition.

#### References

1. V. Velikov, S. Borick, C. A. Angell, *Science* **294**, 2335 (2001).
2. O. Mishima, H. E. Stanley, *Nature* **396**, 329 (1998).
3. C. A. Angell, *Proc. Natl. Acad. Sci. U.S.A.* **92**, 6675 (1995).
4. M. G. Sceats, S. A. Rice, in *Water: A Comprehensive Treatise*, F. Franks, Ed. (Plenum, London, 1982), vol. 7, pp. 83–211.
5. O. Mishima, L. D. Calvert, E. Whalley, *Nature* **310**, 393 (1984).
6. E. Mayer, *J. Appl. Phys.* **58**, 663 (1985).
7. Y. P. Handa, D. D. Klug, *J. Phys. Chem.* **92**, 3323 (1988).
8. G. P. Johari, *J. Phys. Chem. B* **102**, 4711 (1998).
9. J. S. Tse *et al.*, *Nature* **400**, 647 (1999).
10. G. P. Johari, A. Hallbrucker, E. Mayer, *Science* **273**, 90 (1996).
11. K. Ito, C. T. Moynihan, C. A. Angell, *Nature* **398**, 492 (1998).

#### PERSPECTIVES: PHYSIOLOGY

## A One-Domain Voltage-Gated Sodium Channel in Bacteria

William A. Catterall

Learning, memory, movement, sensation, and other complex processes are all coordinated by electrical signals (action potentials) conducted along the long fibers of nerve cells. In both multicellular animals and complex single-cell organisms such as the eukaryote *Paramecium*, electrical signals are generated locally and action potentials are conducted globally through the activity of a family of voltage-gated sodium channels. This ion channel family was not thought to exist in bacteria, the jellyfish being the simplest organism in which it had been found (1). On page 2372 of this issue, Ren *et al.* (2) surprise us with their discovery of the first

voltage-gated ion channel in a prokaryote. They describe the structure and function of a sodium channel in the salt-loving bacterium *Bacillus halodurans*.

The voltage-gated sodium ( $\text{Na}_v$ ) channels of eukaryotes are complex proteins composed of more than 2000 amino acid residues. The large pore-forming  $\alpha$  subunit comprises four homologous domains containing six transmembrane  $\alpha$  helices (see the figure) (3). It is bell-shaped (4) and associates with smaller  $\beta$  subunits (3). As Ren *et al.* report (2), the bacterial sodium channel (NaChBac) is much simpler, consisting of a single domain with 274 amino acid residues and six transmembrane  $\alpha$  helices (see the figure). This structure resembles voltage-gated potassium ( $\text{K}_v$ ) channels, which are homotetramers (composed of four identical

subunits) (5). The primary structure of NaChBac raises provocative questions about the three most important tasks of sodium channels—selective ion conductance, voltage-dependent activation, and fast inactivation.

In vertebrates, an ion selectivity filter enables voltage-gated sodium channels to conduct sodium ions 15 to 50 times as rapidly as potassium and calcium ions, the other prevalent cations in physiological fluids (6). The transmembrane pore of these ion channels is formed by the S5 and S6 segments of the  $\alpha$  subunit and the pore loop segment between them [reviewed in (3)]. Ion selectivity is thought to be determined by a small number of amino acid residues in the second half of the pore loop, which forms a narrow opening into the extracellular end of the pore (7). As discussed by Ren *et al.* (2), preferential sodium selectivity in  $\text{Na}_v$  channels is thought to require an asymmetric pore structure with different amino acid residues in key positions in the pore loops of each of the four domains. At one critical position, the amino acid residues in the pore loops of the four domains of

The author is in the Department of Pharmacology, University of Washington, Seattle, WA 98195, USA. E-mail: wcatt@u.washington.edu

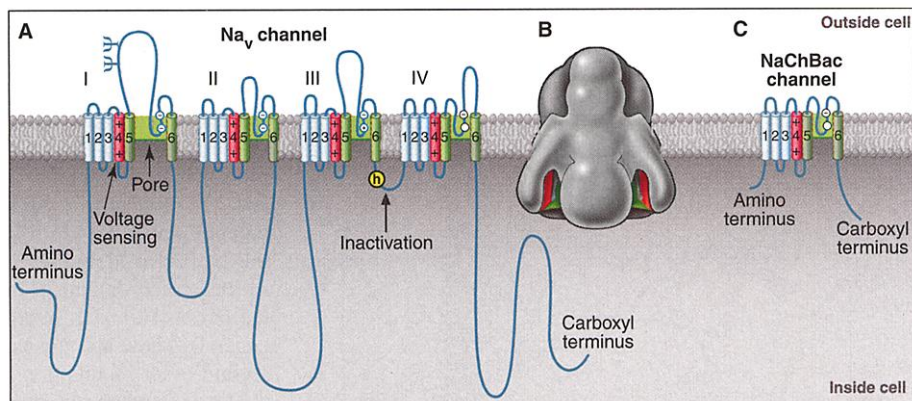
$\text{Na}_v$  channels are aspartate, glutamate, lysine, and alanine (DEKA). Evidence from mutagenesis experiments indicates that these four residues must be different from each other so that they can form an asymmetric ion selectivity filter, which selects sodium ions over calcium ions (7, 8). In light of these previous results, it is surprising that the NaChBac channel, expressed in bacteria as a homotetramer with glutamate residues in the key position in all four pore loops (EEEE), has such high sodium selectivity. This finding implies either that the homotetramer can form an asymmetric pore structure (by arranging identical subunits in an asymmetric assembly) or that asymmetry of the pore structure is not really required for sodium

charges primarily by combining rotation and rearrangement of the surrounding protein to expose the positive charges to the extracellular medium with only small outward movement (14).

Fast inactivation during prolonged depolarization is the third key property of  $\text{Na}_v$  channels, allowing them to close and return to the resting state within 1 ms, as required for generation of action potentials at high frequency. Impairment of this process by mutation causes inherited diseases of nerve hyperexcitability, such as periodic paralysis, cardiac arrhythmia and epilepsy (17). Inactivation may involve closure of an intracellular inactivation gate formed by the peptide loop connecting homologous domains III and IV, which occludes the intracellular end of the pore (3, 18–21). NaChBac is inactivated like a  $\text{Na}_v$  channel, but more slowly by a factor of 100. Because it is a homotetramer, it has no equivalent of the intracellular loop connecting domains III and IV of the  $\text{Na}_v$  channels.

How is NaChBac inactivated? The single-domain  $\text{K}_v$  channels may provide the answer. These channels are inactivated in two ways at a slow rate comparable to that of NaChBac inactivation. N-type inactivation involves the amino-terminal segment of the  $\text{K}_v$  channel, which folds like a ball and chain into the channel structure and blocks the pore from the inside (like  $\text{Na}_v$  channel inactivation) (22, 23). In contrast, C-type inactivation of the  $\text{K}_v$  channel results from closure of the pore by a mechanism involving the pore loops in all four domains, closure resembling the annular movements of a camera shutter (24, 25). The related slow inactivation of  $\text{Na}_v$  channels may work similarly (26, 27). The amino-terminal domain of NaChBac is far shorter than that of  $\text{K}_v$  channels, and it seems too short to serve as a tethered ball and chain for inactivation. Therefore, it seems most likely that NaChBac uses C-type inactivation to yield concerted closure of the pore by the pore loops in all four domains. The new NaChBac channel now provides an opportunity to explore this poorly understood form of inactivation.

Perhaps the most exciting aspect of NaChBac's discovery is the possibility that it can be expressed in large amounts, crystallized, and analyzed by x-ray crystallography to determine its three-dimensional structure. To date, only the pore region of a related bacterial potassium channel (KcsA) has been analyzed at the structural level (28). It has yielded a wealth of information about how the pore works and maintains potassium ion selectivity. The KcsA channel, however, does not have voltage-dependent gating, thus



**Comparing  $\text{Na}_v$  and NaChBac channels.** (A) Arrangement of the transmembrane  $\alpha$  subunit of the mammalian  $\text{Na}_v1.2$  voltage-gated sodium channel. Note the four-domain structure with six  $\alpha$ -helical transmembrane segments in each domain. The S5 and S6 segments and the pore loop region between them are highlighted in green. The positively charged S4 gating segments are highlighted in red. The inactivation gate and the isoleucine-phenylalanine-methionine (IFM) motif that is crucial for inactivation are highlighted in yellow. (B) The three-dimensional structure of the  $\text{Na}_v$  channel  $\alpha$  subunit at 20 Å resolution, compiled from electron micrograph reconstructions (4). Note the bell shape with most of the mass on the intracellular side of the membrane and a cap over the extracellular opening of the pore. (C) NaChBac, the bacterial voltage-gated sodium channel. Note the similarity to one domain of the  $\text{Na}_v$  channel  $\alpha$  subunit.

selectivity. Experiments to test this question should help to reveal the mechanism of sodium channel ion selectivity.

The pharmacology of NaChBac's pore region is also unexpected, as it more closely resembles that of voltage-gated calcium ( $\text{Ca}_v$ ) channels. Although NaChBac is not blocked by the traditional sodium channel blocker tetrodotoxin, it is blocked by divalent cations and two different types of calcium channel blockers (2).  $\text{Ca}_v$  channels have four glutamate residues (the EEEE motif) in the key position in the pore loop. These channels conduct sodium ions well in the absence of divalent cations, but sodium conductance is prevented by the presence of calcium ions or other divalent cations (9, 10). Perhaps the EEEE motif of NaChBac, like the similar motif in  $\text{Ca}_v$  channels, is permissive for sodium conductance, whereas other unidentified molecular fea-

tures of the NaChBac pore prevent divalent cation binding and conductance and thereby confer sodium selectivity. The second hallmark property of the voltage-gated ion channel family is steep voltage-dependent opening in response to changes in the electrical potential across cell membranes. Current molecular models of the activation gating process suggest that the S4 transmembrane  $\alpha$  helices in each domain serve as voltage sensors. They contain four to seven positive charges from cationic amino acids (called gating charges), which are positioned at intervals of three residues. Depolarization of the membrane exerts an electrostatic force, pushing the positive charges in the S4 segments in the outward direction

no information about this crucial mechanism of excitation can be gleaned from its structure. With NaChBac—a primordial member of the ion channel gene family—in hand, we can look forward to resolving questions about ion selectivity, voltage-dependent activation, and inactivation at the structural level.

## References

1. P. A. V. Anderson, M. A. Holman, R. M. Greenberg, *Proc. Natl. Acad. Sci. U.S.A.* **90**, 7419 (1993).
2. D. Ren *et al.*, *Science* **294**, 2372 (2001).
3. W. A. Catterall, *Neuron* **26**, 13 (2000).
4. C. Sato *et al.*, *Nature* **409**, 1047 (2001).
5. L. Y. Jan, Y. N. Jan, *Annu. Rev. Neurosci.* **20**, 91 (1997).
6. B. Hille, *Ionic Channels of Excitable Membranes* (Sinauer Associates, Sunderland, MA, ed. 2, 1992).
7. S. H. Heinemann *et al.*, *Nature* **356**, 441 (1992).
8. I. Favre, E. Moczydlowski, L. Schild, *Biophys. J.* **71**, 3110 (1996).
9. P. Hess, R. W. Tsien, *Nature* **309**, 453 (1984).
10. E. W. McCleskey, W. Almers, *Proc. Natl. Acad. Sci. U.S.A.* **82**, 7149 (1985).
11. W. A. Catterall, *Annu. Rev. Biochem.* **55**, 953 (1986).
12. H. R. Guy, P. Seetharamulu, *Proc. Natl. Acad. Sci. U.S.A.* **83**, 508 (1986).
13. N. Yang, R. Horn, *Neuron* **15**, 213 (1995).
14. A. Cha, G. E. Snyder, P. R. Selvin, F. Bezanilla, *Nature* **402**, 809 (1999).
15. K. S. Glauner, L. M. Mannuzzo, C. S. Gandhi, E. Y. Isacoff, *Nature* **402**, 813 (1999).
16. C. Gonzalez, E. Rosenman, F. Bezanilla, O. Alvarez, R. Latorre, *Proc. Natl. Acad. Sci. U.S.A.* **98**, 9617 (2001).
17. F. Lehman-Horn, K. Jurkat-Rott, *Physiol. Rev.* **79**, 1317 (1999).
18. P. M. Vassilev, T. Scheuer, W. A. Catterall, *Science* **241**, 1658 (1988).
19. J. W. West *et al.*, *Proc. Natl. Acad. Sci. U.S.A.* **89**, 10910 (1992).
20. G. Eaholtz, T. Scheuer, W. A. Catterall, *Neuron* **12**, 1041 (1994).
21. C. A. Rohl *et al.*, *Biochemistry* **38**, 855 (1999).
22. T. Hoshi, W. N. Zagotta, R. W. Aldrich, *Science* **250**, 533 (1990).
23. W. N. Zagotta, T. Hoshi, R. W. Aldrich, *Science* **250**, 568 (1990).
24. T. Hoshi, W. N. Zagotta, R. W. Aldrich, *Neuron* **7**, 547 (1991).
25. E. M. Ogjelska *et al.*, *Biophys. J.* **69**, 2449 (1996).
26. H. Todt, S. C. Dudley, J. W. Kyle, R. J. French, H. A. Fozzard, *Biophys. J.* **76**, 1335 (1999).
27. B. H. Ong, G. F. Tomaselli, J. R. Balse, *J. Gen. Physiol.* **116**, 653 (2000).
28. D. A. Doyle *et al.*, *Science* **280**, 69 (1998).

## PERSPECTIVES: PALEOCLIMATE

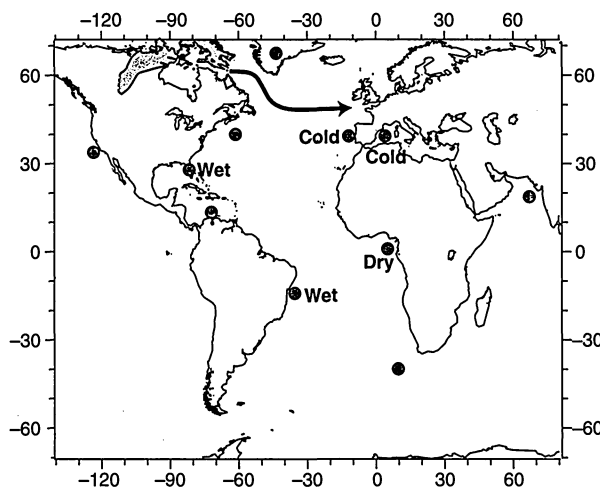
## Climate Swings Come into Focus

Wally S. Broecker and Sidney Hemming

Over the past million years, Earth climate has experienced large-scale oscillations between glacial and interglacial conditions. Increasing evidence from ice cores and marine and terrestrial sediment cores shows that during glacials, climate was extremely variable on a millennial time scale. But not all the data fit into one neat pattern, as the study of the so-called Heinrich events illustrates.

In 1988, Heinrich observed six discreet layers of sediment rich in ice-rafted debris in a deep-sea core from the eastern North Atlantic. The oldest layer was located near the beginning of the last glacial period and the youngest close to the onset of the last deglaciation. Heinrich postulated that these layers had been deposited from melting icebergs (1). Four years later, confirmation of the existence of these layers created interest in their mode of origin (2). The layers are several meters thick in the Labrador Sea but get progressively thinner to the east, reaching a thickness of just 1 to 2 cm by 10°W (3, 4). Measurements of lead isotopes in feldspar grains (5) and of argon isotope ratios in amphiboles (6) pinpointed the source of the rock fragments to be the Canadian shield's Churchill Province (see the first figure). Further support for this source region is provided by the presence of 20 to 30% detrital calcium carbonate, which originates in the limestone that underlies Hudson Bay and Hudson Strait (2, 4, 7).

MacAyeal (8) was quick to suggest a binge-purge hypothesis. As the Laurentide



**Spatial patterns of climate change events.** Sites where the climatic impacts of Heinrich events dominate are indicated with blue dots; sites where those of DO events dominate are indicated with red dots. The black arrow shows the pathway followed by the ice armadas, the green patch is the area where Churchill Province crystalline rocks outcrop, and yellow indicates the limestone underlying Hudson Bay and Strait.

Ice Sheet, which covered much of north America during glacials, thickened in the region of Hudson Bay, geothermal heat gradually warmed its base until melting occurred. Guided by the soft sediment underlying Hudson Bay and Hudson Strait, the ice whooshed out into the Labrador Sea. From there, it was transported by the prevailing currents and winds eastward across the Atlantic (see the first figure). The great armadas of icebergs melted along the way, dropping debris to the sea floor. Once the deluge exhausted itself, the ice sheet once again began to thicken,

initiating another cycle. This hypothesis is consistent with the 10<sup>4</sup>-year spacing of these events because 2 to 3 km of ice could accumulate in this time.

Heinrich events are not the only prominent climate cycles. The millennial duration Dansgaard-Oeschger (DO) events are recorded in Greenland ice

and in a number of detailed paleoclimate records from the Northern Hemisphere.

In these records and in the ice cores, Heinrich events generally show up only as a second-order modulation of the timing and amplitude of the DO events (7), although a few published records do show Heinrich impacts that are more prominent than DO impacts. For example, the pollen record in Florida's Lake Tulane reveals alternating pine and oak episodes geared to the Heinrich-event timing (9).

A sediment core from Brazil's continental margin shows a large pulse of continental debris for each Heinrich event (10). And a Chinese loess record shows intensified winter monsoons that correlate with

Heinrich events (11). A sediment record from the Arabian Sea off Pakistan shows both DO and Heinrich impacts (see the second figure) (12).

DO events are widely believed to be triggered by reorganizations of the thermohaline circulation related to the Atlantic's salt balance. Why do the massive inputs of fresh water generated by the melting of the ice armadas during Heinrich events not produce more noticeable climatic impacts?

Participants at a recent miniconference on Heinrich events at Lamont-Doherty

The authors are in the Lamont Doherty Earth Observatory, Columbia University, Palisades, NY 10964, USA. E-mail: broecker@ldeo.columbia.edu